2014

# Collagen attachment to the substrate controls cell clustering through migration

Yue Hou
*Iowa State University*

Laura L. Rodriguez
*Iowa State University*

Juan Wang
*Iowa State University*, juanw@iastate.edu

***See next page for additional authors***

# Collagen Attachment to the Substrate Controls Cell Clustering through Migration

Yue Hou[1], Laura Lara Rodriguez[1], Juan Wang[1] and Ian C. Schneider[1,2*†]

[1]Department of Chemical and Biological Engineering, Iowa State University

[2]Department of Genetics, Development and Cell Biology, Iowa State University

*Present address: Iowa State University, Department of Chemical and Biological Engineering, 2114 Sweeney Hall, Ames, IA, 50011-2230

[†]Author for correspondence (phone: (515) 294-0450, fax: (515) 294-2689, e-mail: ians@iastate.edu)

This is a manuscript of an article from Physical Biology 11 (2014): 056007, doi: 10.1088/1478-3975/11/5/056007.
Posted with permission.

## ABSTRACT:

Cell clustering and scattering play important roles in cancer progression and tissue engineering. While the extracellular matrix (ECM) is known to control cell clustering, much of the quantitative work has focused on the analysis of clustering between cells with strong cell-cell junctions. Much less is known about how the ECM regulates cells with weak cell-cell contact. Clustering characteristics were quantified in rat adenocarcinoma cells, which form clusters on physically adsorbed collagen substrates, but not on covalently attached collagen substrates. Covalently attaching collagen inhibited desorption of collagen from the surface. While changes in proliferation rate could not explain differences seen in the clustering, changes in cell motility could. Cells plated under conditions that resulted in more clustering had a lower persistence time and slower migration rate than those under conditions that resulted in less clustering. Understanding how the ECM regulates clustering will not only impact the fundamental understanding of cancer progression, but also will guide the design of tissue engineered constructs that allow for the clustering or dissemination of cells throughout the construct.

This is a manuscript of an article from Physical Biology 11 (2014): 056007, doi: 10.1088/1478-3975/11/5/056007.
Posted with permission.

## INTRODUCTION:

Tissues reorganize continuously by disassembling and assembling cellular structures. The disassembly process is often referred to as scattering and describes the well-studied epithelial to mesenchymal (EMT) transition [1]. The assembly process is often referred to as aggregation or clustering. Both cell scattering and clustering play important roles in pathologies like cancer metastasis [2], but also in regenerative medicine and tissue engineering [3]. In carcinomas, the primary tumor develops as cluster of cells from an epithelial layer, where cells are attached. Mutations in oncogenes disrupt cell-cell adhesion [4], causing cells to break off the primary tumor as single cells or clusters, metastasize to distant organs and form nascent secondary tumors [2]. Clustering during metastasis might also be advantageous. For example, squamous cell carcinomas can escape apoptosis by forming multicellular clusters [5, 6]. Some cancer cells also undergo EMT, where epithelial cells lose polarity and diminish cell-cell adhesion, and gain migratory and invasive properties of mesenchymal cells [7]. In addition to pathological *in vivo* environments, engineered environments must be able to orchestrate cell scattering and clustering during the formation of functional tissues [3]. Many types of cells are known to self-assemble into organ-like structures in engineered environments outside of the body [8-10]. For instance, mouse embryonic cells from submandibular gland can assemble into branched structures that resemble salivary gland buds *in vitro* [8]. While cell clustering is desired for certain specific tissue engineering applications, other applications require limiting cell clustering, particularly in the case of stem cell expansion [11]. Understanding the mechanisms that contribute to scattering and clustering will not only provide therapeutic targets for pathologies, but also will guide the design of engineered tissue environments that can regulate the degree of cell scattering and clustering.

In the most general sense, scattering is the process by which cells transit from a state of close proximity to a state where cells are well-dispersed. In most studies, the cells in close proximity form cell-cell junctions, so scattering is described as a disassembly process that includes loss of cell-cell junctions [1]. This type of scattering can proceed either through transcriptional control, usually by

This is a manuscript of an article from Physical Biology 11 (2014): 056007, doi: 10.1088/1478-3975/11/5/056007.
Posted with permission.

altering the expression of the cell-cell adhesion molecule E-cadherin [12, 13], or through signaling [14, 15] or cytoskeletal [16, 17] events, usually by altering the relative magnitudes of the cell-cell or cell-substrate adhesion forces. Numerous extracellular ligands such as hepatocyte growth factor [18] or epidermal growth factor [14, 19] can induce scattering. In addition to these chemical inputs, mechanical inputs, such as the stiffness of the substrate can regulate traction force and determine whether cells scatter [20]. Clustering, on the other hand, is the process by which cells transit from a well-dispersed state to a state of close proximity. Cell clustering can be induced by extracellular ligands like insulin like growth factor [21] or through force mediated between attached cells [22, 23]. Again, in most studies the cells in close proximity form cell-cell junctions, so clustering is described as an assembly process that includes formation of cell-cell junctions. When cell-cell adhesion is significant and in the absence of proliferation, the assembly of clusters can result either from random migration [8, 24-27], paracrine-mediated directed migration [28, 29] or mechanically-induced cell compaction [23]. All three induce cell-cell contact and cluster formation when cells collide [30]. In the presence of proliferation, the continual division of well-attached daughter cells can also act to enhance clustering [31]. While cell clustering brought on by cell-cell adhesion is viewed as the more common mechanism that brings about clustering, it is important to realize that cells lacking the ability to make significant cell-cell contact can cluster too. These mechanisms include proliferation coupled with slow migration [32], paracrine-mediated attraction of cells or perhaps mechanically-induced cell compaction [20]. Determining which mechanisms are at play in specific systems will allow for approaches to control cell clustering.

Since migration, cell-substrate adhesion and perhaps proliferation are important processes in the disassembly and assembly of cell clusters, the ECM plays a role in regulating scattering and clustering [16, 25, 33, 34]. The ECM determines the speed and persistence of cell migration, which can act to cluster cells [25]. It also sets the cell-substrate adhesive force, so the type of the ECM ligand and its mechanical stiffness are important regulators of cell scattering [16, 23, 35]. For example, epithelial cell scattering is enhanced on collagen and fibronectin, as compared with laminin 1 and rigid substrates that

This is a manuscript of an article from Physical Biology 11 (2014): 056007, doi: 10.1088/1478-3975/11/5/056007.
Posted with permission.

produce high traction forces promoted scattering, in comparison to more compliant substrates [16, 23]. In addition, cell clustering is also enhanced in environments where cells can exert large contractile forces [36-38]. These contractile forces coupled with matrix degradation act to remodel the ECM [39], which in turn can either enhance scattering or clustering.

While there have been several recent quantitative efforts made to characterize scattering and clustering on different ECM [16, 25], this has mainly focused on cells that can generate strong cell-cell junctions. We were interested in probing environmental determinants that lead to the clustering of cells that lack robust cell-cell junctions. Therefore, we constructed four types of substrates that varied in way in which collagen was attached to the surface and in their adhesivity. A rat adenocarcinoma cell line (MTLn3) was used as a model system to study scattering and clustering in cells that lack strong cell-cell adhesion. We developed a method to quantify the clustering and found higher clustering on physically adsorbed collagen substrates than on covalently attached substrates. Higher clustering correlated with substrates where the collagen was not stably attached and desorbed from the surface. No significant difference in cell proliferation was observed between the conditions. However, cell migration was enhanced on collagen that was covalently attached to the surface. This indicates that the attachment mechanism of collagen can alter the clustering behavior of cells by regulating the migration rate. These results have importance in understanding how matrix remodeling might alter clustering *in vivo*, but also how the immobilization of ECM in engineered constructs is a critical factor in disseminating cells across a surface or throughout a matrix.

This is a manuscript of an article from Physical Biology 11 (2014): 056007, doi: 10.1088/1478-3975/11/5/056007.
Posted with permission.

## METHODS:

### Materials:

Cell culture media was α-MEM medium (Life Technologies, Grand Island, NY, USA) containing 5 % fetal bovine serum (Life Technologies, Grand Island, NY, USA) and 1 % penicillin-streptomycin (Life Technologies, Grand Island, NY, USA). Collagen (Col) and poly-L-lysine (PLL) solution contained rat tail collagen I (Life Technologies, Grand Island, NY, USA) and poly-L-lysine hydrochloride (Sigma-Aldrich, St. Louis, MO, USA) and was dissolved in UV-sterilized 0.5 M acetic acid (Fisher Scientific, Hampton, New Hampshire, USA). Imaging media was α-MEM medium without phenol red containing 5 % fetal bovine serum, 1 % penicillin-streptomycin, and 12 mM HEPES (Fisher Scientific, Hampton, New Hampshire, USA). The matrix metalloproteinase inhibitor, GM6001 (Calbiochem, EMD Millipore Corporation, Billerica, MA, USA) was prepared at 10 μM and dissolved in Dulbecco's Phosphate-Buffered Saline (DPBS) with calcium and magnesium (Life Technologies, Grand Island, NY, USA).

### Cell Culture:

Rat mammary adenocarcinoma cell line (MTLn3) was obtained from Dr. Jeffrey E. Segall (Albert Einstein College of Medicine). Cells were maintained in cell culture media at 37 °C in 5 % $CO_2$ and were passed every two or three days.

### Collagen Substrate Treatment:

No. 1 1/2-22 mm square coverslips (Corning Inc., Corning, New York, USA) were sonicated 30 minutes in the following solutions to make squeaky clean coverslips: hot tap water with Versa Clean detergent (Fisher Scientific, Hampton, New Hampshire, USA), hot tap water, distilled water, double distilled water, 1 mM EDTA solution (Fisher Scientific, Hampton, New Hampshire, USA), 70% ethanol in water and 100% ethanol. An adaptation of a protocol to functionalize coverslips with glutaraldehyde was used

This is a manuscript of an article from Physical Biology 11 (2014): 056007, doi: 10.1088/1478-3975/11/5/056007.
Posted with permission.

[40, 41]. Cleaned coverslips were soaked in a 3:1 sulfuric acid (Fisher Scientific, Hampton, New Hampshire, USA):30% hydrogen peroxide (Fisher Scientific, Hampton, New Hampshire, USA) solution for one hour, washed with double distilled water and placed in 10 mL of 1% aminopropyltriethylsilane (APTES) (Fisher Scientific, Hampton, New Hampshire, USA) in 10 mM acetic acid for two hours. They were then rinsed with double distilled water, spin dried and heat-treated in an oven at 100 ºC for one hour. Finally, the coverslips were treated with 5 mL of 6% glutaraldehyde (Fisher Scientific, Hampton, New Hampshire, USA) in phosphate buffered saline (PBS) without calcium and magnesium (Gibco, Grand Island, New York, USA) for two hours. The functionalized coverslips were stored in double distilled water at 4 ºC until use. A 1.8 μg/mL Col solution with or without 2 μg/mL PLL was added onto a 35 mm cell culture dish (Fisher Scientific, Hampton, New Hampshire, USA) and covered either by a cleaned coverslip or a functionalized coverslip. Alternatively, collagen was printed onto the surface. Flat polydimethylsiloxane (PDMS) stamps were made by mixing 184 Silicone Elastomer Base (Dow Corning) with its curing agent in a 10:1 weight ratio and then allowing it to spread on top of a fused silica master. The master coated with PDMS was exposed to a vacuum to remove any air pockets and then cured for an hour at 60 °C. PDMS stamps were sonicated in double distilled water and in 100% ethanol. A 200 μL collagen solution of 75 μg/mL collagen I and 25 μg/mL Alexa Fluor 555-labeled collagen I in 0.5 M acetic acid was applied to each stamp. After 40 min incubation, the collagen solution was removed and then the stamp was placed on the functionalized coverslip and allowed to incubate for fifteen minutes. Later, the stamp was removed and the coverslips were incubated in the dark for 2 hours. Before seeding MTLn3 cells, the coverslips were washed with PBS.

## Clustering Assay:

MTLn3 cells between passage 2 and 20 were seeded onto Phys-COL or Cov-COL substrates in 35 mm cell culture dishes at an approximate density of 50,000 cells per dish and maintained in cell culture media at 37 °C in 5 % $CO_2$. Dishes with cells were imaged every 8 hours from 0 hour to 48 hours. Phase

contrast images were captured at 10× magnification (NA 0.50, Nikon) with a charge-coupled device (CoolSNAP HQ2, Photometrics) attached to an inverted microscope (Eclipse Ti, Nikon) run by μManager [42]. Cell centroids were identified manually by MTrackJ plugins of ImageJ. Clustering was quantified in MATLAB (The MathWorks, Natick, MA) using a radial distribution function (RDF) and a *k*-means clustering analysis. The peak and decay distance of cells were calculated using the MATLAB function `rdfcalc` (from GUI: Radial Distribution Function, File ID: #31494, File exchange, MATLAB CENTRAL). The peak distance ($R_{max}$) is the distance that resulted in the highest probability. The decay distance ($R_{1/2max}$) is the distance where the probability equals the half height of the peak occurs in a region of the RDF that is most sensitive to changes in scattering. The cell number in clusters and percentage of cells in clusters were quantified based on the identified clusters and total cell number. Clusters were identified using a *k*-means clustering approach. Briefly, if the centroid of a cell was greater than 26 μm from every other cell centroid, this cell was defined as single cell and its centroid was deleted from the centroid matrix used by the *k*-means clustering algorithm. After this first cut, clusters were identified using the `kmeans` function in MATLAB. Cluster number was determined by an iterative process of calculating the percentage of variance. The percentage of variance is defined as the between cluster variance divided by the total variance. However, the between cluster variance is simply equal to the total variance minus the within cluster variance, and consequently, the percentage variance is governed by the following equation:

$$\%Var = 1 - \frac{\frac{\sum_{i=1}^{N_{cell}} D^2{}_{i,cell-cluster}}{N_{cell}}}{\frac{\sum_{j=1}^{N_{cell}}\sum_{k=1}^{N_{cell}} D^2{}_{jk,cell-cell}}{N^2{}_{cell}}}, \qquad (1)$$

This is a manuscript of an article from Physical Biology 11 (2014): 056007, doi: 10.1088/1478-3975/11/5/056007.
Posted with permission.

where $D_{i,cell\text{-}cluster}$ is the cell centroid to cluster centroid distance, $N_{cell}$ is the number of cells in each image and $D_{jk,cell\text{-}cell}$ is the distance between cell centroids. The numerator is the within cluster variance and the denominator is the total variance. Cluster number was tested from two to $N_{cell}$ and the percentage of variance was calculated. When the percentage of variance reached a target, the iteration stopped and that cluster number was the set as the final cluster number. Qualitatively, clusters were split or merged if the percentage of variance target was set too high or low, respectively. However, choosing a percentage of variance between 0.9 and 0.9995 did not change the qualitative differences between physically adsorbed and covalently linked collagen, even though the quantitative values of the mean cell number in clusters was different. Consequently, a value of 0.995 was chosen.

## Collagen Degradation and Uptake Assay

Collagen was labeled using Alexa Fluor 555 carboxylic acid, succinimidylester (Life Technologies, Grand Island, NY, USA) and was attached to the surface at a concentration of 1.8 μg/mL. For substrates with cells, MTLn3 cells in imaging media were then flowed into this chamber at an approximate density of 25,000 cells per coverslip. For substrates with cells plus GM6001, 0.25 μM GM6001 solution was added into the chamber. For substrates without cells, only the imaging media was flowed into the chamber. The chambers were then sealed with VaLaP and imaged on a heated stage. For the degradation assay, differential interference contrast (DIC) images were captured at 0, 6 and 24 hours using a 40x oil objective (*NA* 1.30, Nikon, Melville, NY, USA) using the same imaging system as mentioned above. Epifluorescence (EPI) images were captured at 0, 6 and 24 hours using the same objective with an excitation filter ET555/25x and an emission filter ET605/52m (Chroma). The fluorescence intensity of the whole image was quantified using ImageJ. Collagen density was quantified by drying a drop of a known volume of collagen solution and measuring the fluorescence under the same conditions as the experiments. The specific fluorescence for Cov-COL and Phys-COL surfaces was estimated as being 0.1-0.5 (#/μm$^2$)/a.u. This places the range on initial collagen coverage at 200-1000 #/μm$^2$ for Phys-COL

This is a manuscript of an article from Physical Biology 11 (2014): 056007, doi: 10.1088/1478-3975/11/5/056007.
Posted with permission.

and 100-500 #/$\mu m^2$ for Cov-COL. For the uptake assay, MTLn3 cells were incubated for 6 h in cell culture media at 37 °C in 5 % $CO_2$, mounted into the chambers and time lapse images were taken using the same imaging system as mentioned above. DIC images were captured every two minutes, while EPI images were taken every two hours. The cells were manually selected according to the DIC images and then the fluorescent intensity of the cells was quantified based on the EPI images using ImageJ.

## Cell Migration Assay

The cell migration assay was performed based on the previous work [43]. Briefly, MTLn3 cells were incubated on 3μg/mL collagen substrates for 6 h and were mounted into perfusion chambers (Warner Instruments, Hamden, CT, USA) in imaging media. Chambers were imaged on an automated heating stage every 2 minutes for 12 hours. Phase contrast images were captured at 10x objective (*NA* 0.30, Nikon) using the same imaging system as mentioned above. Cell centroids were identified manually by MTrackJ plugins of ImageJ. Instantaneous cell speed was calculated by measuring the cell displacement and dividing it by the time interval, 2 minutes. This value was averaged over the entire timelapse for all cells under one condition. The average mean-squared displacement (MSD) was calculated using all the cells from one condition. These data can be fitted a persistence random walk model [44-46],

$$\left\langle d^2(t)\right\rangle = nS^2P\left[t - P\left(1 - e^{-t/P}\right)\right]. \qquad (2)$$

using a nonlinear least square regression analysis to yield a model speed, *S*, and model persistence time, *P*. As the time lag, *t*, grows large the asymptotic behavior shows that the slope defines the random motility coefficient, *D* and is governed by the following equation:

$$D = nS^2P\,, \qquad (3)$$

Where $n$ is the number of dimensions and $S$ and $P$ are defined as above. The random motility coefficient, $D$, can either be calculated using Eqn. 3 after the nonlinear fit or by fitting the MSD curves at long times with a linear equation. Both approaches yielded similar results.

## Immunofluorescence and Adhesion Analysis

Cells were fixed using paraformaldehyde, permeabolized with triton-X and stained with alexa 488-phalloidin (Life Technologies), mouse anti-paxillin (349, BD Biosciences) and a donkey-anti mouse Cy5 antibody (Jackson ImmunoResearch) as described elsewhere [47]. Images of focal adhesions were taken using a 60x objective (*NA* 1.49, Nikon) under epifluorescence illumination. Adhesions were quantified using image-processing tools on ImageJ as follows. A rolling ball background subtraction algorithm was used, followed by a median filter. A histogram of gray values for pixels in the resulting image was obtained and plotted on a logarithmic scale. The gray value corresponding to the change in slope of the histogram was used to select the threshold gray value to identify areas of the image that correspond to adhesions. A binary operation was applied using the threshold gray value. Adhesion integrated intensity (area x mean gray value), number of adhesions per cell and adhesion area were quantified for each condition.

## RESULTS:

### Mechanism of collagen attachment regulates cell clustering

Collagen is a large charged protein that can physically adsorb to bare surfaces (Phys-COL) or covalently react with functionalized surfaces (Cov-COL). Both approaches are commonly used to render glass coverslips or other surfaces adhesive towards cells. We observed that these different collagen attachment mechanisms altered the clustering behavior of a rat adenocarcinoma cell line (MTLn3). MTLn3 cells adhered to Phys-COL substrates and formed noticeable clusters after 8 h (figure 1(*a*)); whereas those adhered to Cov-COL substrates did not cluster as tightly (figure 1(*b*)). Interestingly, this clustering was not due to cell-cell contact as in other epithelial cells, because MTLn3 cells are highly metastatic and do not form cell-cell contacts. We were interested in quantifying the clustering, so we logged the position of the nucleus of each cell (figure 2 (*a*) and (*b*)). A radial distribution function (RDF) was calculated from the positional data (figure 2(*c*)). The RDF describes the probability of finding a cell at a distance from a given reference cell. In addition, a *k*-means clustering algorithm was used to identify clusters. These two quantitative approaches formed the basis of our analysis. Different parameters, peak distance ($R$) and decay distance ($R_{1/2max}$) were calculated from the RDF (figure 2(*c*)). Larger $R$ and $R_{1/2max}$ values indicate more scattered and less clustered cells. To complement this data, the percentage of cells in clusters was calculated from the *k*-means clustering analysis.

Since cells were less clustered on Cov-COL surface, but appeared to spread more quickly (figure 1), we decided to examine whether the clusters were caused by differences in non-specific adhesivity of the substrate. Therefore, we added an adhesive component, poly-L-lysine (PLL), to both substrates and observed cell morphologies on the four different substrates: Phys-COL, Cov-COL, Phys-COL+PLL and Cov-COL+PLL (figure 3). Moderate differences were seen in the cell spreading area over time between Phys-COL and Cov-COL, but PLL did not seem to dramatically impact cell spreading (figure S1). Cells on Phys-COL substrates formed tighter clusters and were less spread than cells on Cov-COL substrates

This is a manuscript of an article from Physical Biology 11 (2014): 056007, doi: 10.1088/1478-3975/11/5/056007.
Posted with permission.

(figure 3 and S1). The PLL treatment only marginally altered the clustering (figure 3). In order to support these qualitative observations, we quantitatively analyzed the clustering behavior using the approaches described above.

To quantify the clustering behavior on the four different substrates, we measured peak distance ($R$), decay distance ($R_{1/2max}$), cell number in clusters, percentage of cells in clusters, RDF of cells and RDF of clusters over time (figures 4, S2 and S3). Clear differences were seen. Enhanced clustering on physically adsorbed collagen resulted in smaller values of both $R$ and $R_{1/2max}$ (figure 4(*a*) and (*d*)) and a larger mean cell number in clusters (figure 4(*b*)). Finally, the most dramatic difference was seen in the percentage of cells that existed in clusters. After 8 h, the percentage of cells in clusters on covalently attached collagen decreased by roughly 50% over the next 16 h, whereas the percentage of cells in clusters on physically adsorbed collagen remained constant (figure 4(*c*)). The difference in either mean cluster size or percentage of cells in clusters between physically adsorbed collagen and covalently attached collagen is shown in figures 4(*e*) and (*f*) and appears to be maximal at or after 16 h. In addition, a comparison of the distributions shows that physically adsorbed collagen produces fewer single cells and more 2-, 3- and 4-cell clusters at 16 and 32 h (figure 4(*g-f*)). These data suggest that the largest effect on clustering was the mechanism of attachment of collagen, with a smaller effect due to the non-specific adhesivity of the substrate.

## Covalent collagen attachment inhibits desorption and uptake by cells

Given that collagen attachment to the surface drives clustering, we were interested in determining if the surface coverage of collagen was different between conditions and whether it changed over time. To determine this, we used Alexa Fluor 555-labeled collagen to construct Phys-COL and Cov-COL substrates and quantified the fluorescent intensity of the whole image over time. We examined substrates with and without cells. However, because MTLn3 cells are known to express matrix

metalloproteinases (MMPs), which could cleave and potentially release collagen from the surface, we also treated cells with a broad spectrum MMP inhibitor, GM6001. Although the bulk concentrations of fluorescent collagen used to treat both substrates were the same, the fluorescence on the Phys-COL substrates was approximates two-fold larger than that on Cov-COL substrates (figure 5). Collagen fluorescence on the Phys-COL substrates decreases dramatically over time, which is interesting, given the common use of this protocol (figure 5(*a*)). Some of this decrease is inhibited by GM6001 at 6 hr but most occurs even in the absence of cells, indicating that collagen desorption is the largest contributor to the fluorescence decrease as compared to blocking enzymatic cleavage of collagen. Cov-COL substrates differ. Under no condition does the fluorescence decrease. In the absence of cells, fluorescence remains constant. When cells are present, but proteinase activity is inhibited with GM6001, fluorescence is moderately higher, but not statistically significantly higher. When cells are present and proteinase activity is not inhibited, fluorescence actually increases. However, closely packed fluorophores on proteins are known to quench, generating enhanced fluorescence [48]. While our dye to protein ratio is 2, below a ratio that induces robust quenching (> 5), it is possible that close packing and covalent attachment to the surface places dyes in close proximity. This would result in 1) a lower initial fluorescence than Phys-COL and 2) an increase in fluorescence in response to proteinases released from cells, consistent with results shown in figure 5(*b*).

Another approach to quantify the amount of collagen that desorbs from the surface is to measure the uptake of fluorescent collagen by the cells. To investigate how much collagen is taken up after cleavage or desorption from the surface, we imaged cells on the four different substrates with fluorescently labeled collagen and quantified the mean fluorescent intensity of the cells on four substrates over time. The fluorescent intensity of the cells on physically adsorbed collagen substrates was higher than the surrounding areas, while the fluorescent intensity of the cells on covalently attached substrates did not differ from the surrounding area (figure 6).The intensity of collagen inside the cells was quantified and increased with time on physically adsorbed collagen substrates (figure 7, (*a*) and (*c*)).

However, cell fluorescence was much more stable on substrates with covalently attached collagen (figure7, (*b*) and (*d*)). This coupled with quantification of collagen on the surface indicate that surfaces with covalent collagen attachment have a higher collagen density and are more resistant to desorption than surfaces with physically adsorbed collagen. This difference in collagen surface coverage contributes to the differences in clustering. However, why do cells exposed to different collagen surface coverage cluster differently?

## Cell proliferation does not explain clustering differences on different substrates

Given that the mechanism of collagen attachment to the surface results in different surface coverage of collagen over time, we were interested in determining whether this had an effect on proliferation. A simple conceptual model for scattering and clustering of cells that interact weakly involves the two processes of production (proliferation) and diffusion (random cell migration). The production rate is characterized by the doubling time which is the average time between cell divisions. When a cell divides, it forms a cluster of two. Unless these two migrate away from each other before the next division, a cluster of four will be formed. The diffusion rate is characterized by two parts: random cell migration speed and persistence. Consequently, scattering will occur for high diffusion rates relative to production rates, whereas clustering will occur for low diffusion rates relative to production rates. Do cells on Phys-COL substrates proliferate at a higher rate than those on Cov-COL substrates causing the increase in clustering? The total cell number over time was quantified on the four different substrates to examine this question. There was no significant difference in normalized total cell number between substrates until 40 h, much after distinctions in clustering arose (figure 8). Therefore, differences in clustering were not caused by differences in cell proliferation rates.

## Cell migration does explain clustering differences on different substrates

Given that proliferation rates were the same among cells plated on collagen attached to substrates through different mechanisms, we wanted to determine if diffusion rates, set by the cell migration speed and persistence time, were the same among different substrates. We tracked cell nuclei over time on Phys-COL and Cov-COL substrates, calculated instantaneous cell migration speed (figure 9(*a*)) and fitted the mean-squared displacement with the long time lag asymptotic solution of a persistent random walk model (figure 9(*b*)). Both the speed and the motility coefficient of MTLn3 cells on Phys-COL were lower than that on Cov-COL (figure 9(*a*) and (*c*)). Given that focal adhesion and cytoskeleton structure is related to cell migration, we examined these features using immunofluorescence (figure 10). The adhesion number and integrated intensity was about the same (figure 10 (*b*) and (*c*)). However, the F-actin cytoskeleton was organized into brighter, thicker bundles and paxillin staining revealed larger, more stable focal adhesions on Phys-COL substrates as compared with Cov-COL substrates (figure 10 (*a*) and (*d*)). These features are commonly seen in slower migrating cells and are in line with our migration data. The decrease in motility coefficient results in a lower diffusion rate for cells plated on Phys-COL as compared to Cov-COL substrates and leads to enhanced clustering.

## DISCUSSION:

In cells that generate firm cell-cell contact, scattering or clustering is a competition between cell-cell vs. cell-substrate adhesivity [16]. If the cell-cell adhesive force is stronger than the cell-substrate adhesive force, cells will tend to remain clustered as opposed to scattering when contractility increases. If contractility increases dramatically and cells to not detach from each other, retraction will occur [47]. Growth factors or other regulators can initiate scattering by either decreasing the cell-cell adhesive force or increasing the cell-substrate adhesive force. When the ECM is presented under conditions of high cell-substrate adhesion (high concentration and stiffness), cells are more able to scatter in response to stimulants [16]. This is also true for stiff substrates [20, 23], where calculated traction forces have demonstrated that cells pull toward the middle of clusters [22]. In the case of clustering, migration drives the assembly of clusters. Cells from different regions must find each other, so they search for neighbors using a random walk. Consequently, larger clusters are formed when migration rate is maximal [25]. However, in order to cluster cells that form weak cell-cell contact, random migration is not sufficient. With no intercellular adhesion, random migration acts to disperse cells. Consequently, there are only two mechanisms that can explain cell clustering in cells that lack strong cell-cell junctions. The first involves paracrine attraction between cells [28, 29]. Here the paracrine attraction acts as the assembling factor rather than cell-cell adhesion. In addition, high proliferation rates with correspondingly low migration rates could also cause cell clustering. Above we showed that changes in cell clustering correlate with changes in random cell migration. However, can we rule out paracrine attraction in favor of a model that includes only fast proliferation and slow random migration?

Perhaps a scaling approach using parameters that describe the rate of proliferation and dispersion could explain changes in average cell spacing. Others have very elegantly used scaling approaches built upon the wetting of drops on surfaces to describe the increase in both spread area of individual cells [49] and aggregates of cells [50, 51]. However, given that proliferation is a strong feature in the data, we

hesitate to apply this approach. Instead, we prefer to apply an approach that compares the relative importance of proliferation and cell dispersion through migration. This is illustrated in figure 11. Cells are initially somewhat clustered and increase slightly in their clustering over the first 8 h (figure 1 and figure 4 (*b* and *c*)). Moving forward in time from 8 h, several possibilities could exist. If the proliferation and migration rates are nearly zero, the characteristic radius should remain the same. If the proliferation rate is large and the migration rate is nearly zero, the characteristic radius should decrease. If the proliferation rate is nearly zero and the migration rate is large, the characteristic radius should increase. The conditions that we examined in this paper are marked in figure 11 with stars. Because the covalently attached collagen results in a similar proliferation rate, but higher migration rate, the characteristic cluster radius should be higher than that of cells on physically adsorbed collagen. Indeed, this is what we observe (figure 4 (*a* and *d*)).

Proliferation rate is characterized by a first order rate constant, $\mu$ [=] $h^{-1}$. Fits to the time-dependent cell number (figure 8) resulted in rate constants of 0.028 $h^{-1}$ and 0.031 $h^{-1}$ for Cov-Col and Phys-Col substrates, respectively. These equate to doubling times of 25 h and 22 h for Cov-Col and Phys-Col substrates, respectively. It is interesting to note that the point at which the percentage of cells in clusters begins to increase on the Cov-COL substrates is roughly around the doubling time. Dispersion rate or diffusion rate is characterized by a diffusion coefficient, $D$ [=] $\mu m^2/h$. For random migration the diffusion coefficient, $D$ is also referred to as the random motility coefficient and is equal to the migration speed squared multiplied by the persistence time. The random motility coefficient for Cov-Col and Phys-Col substrates is 1200 $\mu m^2/h$ and 340 $\mu m^2/h$, respectively. Given random motility coefficients and proliferation rate constants, the length scale of dispersion is given by the following equation:

This is a manuscript of an article from Physical Biology 11 (2014): 056007, doi: 10.1088/1478-3975/11/5/056007.
Posted with permission.

$$R = \sqrt{\frac{D}{\mu}}. \qquad (4)$$

Consequently, the ratio of dispersion length scales between the Cov-Col and Phys-Col conditions are governed by the following equation:

$$\frac{R_{Cov-Col}}{R_{Phys-Col}} = \sqrt{\frac{D_{Cov-Col}\mu_{Phys-Col}}{D_{Phys-Col}\mu_{Cov-Col}}}. \qquad (5)$$

This ratio can be directly calculated using the $R_{1/2\max}$ for each of the two conditions. The timescale that describes a time after sufficient migration and proliferation have taken place, but before full confluency is 16-40 h. After 40 h, proliferation acts to merge clusters. Between 16-40 h, the ratio given in Eq. 5 was calculated to be ~1.8. Using the random motility coefficient and the proliferation rate constant for both conditions also gives a ratio of 2.0. It is possible that this change in decay distance could be due to differences in spread area, however spread area is not appreciably different among different conditions (figure *S1*). An upper estimate of the difference in spread area is around 1.4 fold, which results in only a 20% change in distance between cell centroids, not the ~ 2 fold change that is seen. This indicates that simple changes in random motility coefficient can explain the quantitative difference in clustering. In addition, it suggests that while paracrine interactions could act to assemble clusters, they are probably not at play here since changes in random motility appear to completely explain the changes in clustering.

The clustering of cells in response to different ECM environments has relevance in cancer. Many clinical and experimental observations suggest that both the weakening of cell-cell contacts and

enhanced migration lead to metastasis driven by single cells [52]. However, others have found less invasive clusters of cells in lymph nodes [53]. This suggests that either multicellular clusters can escape from the primary tissues and form emboli in blood vessels or lymph nodes [54]. The idea that metastases might be in fact multicellular clusters provides motivation for the work showing carcinoma cells can escape suspension-induced apoptosis by forming multicelluar clusters. Single cells in suspension that do not form clusters undergo apoptosis [5, 6]. Moreover, the clustering of stromal cells might be just as important as the clustering of cancer cells as there is some indication that these clusters can initiate tumor invasiveness [55, 56]. Therefore, cell clustering plays an important role in the formation of secondary tumor site by either assembling the cancer cells themselves or reorganizing stromal cells. In addition, a firm understanding of clustering is required in tissue engineering applications. Under certain circumstances clusters might be desired, while other circumstances might require the distribution of cells [3]. The examination of clustering on 2D surfaces does have relevance to tissue engineering. While 3D matrices are the first and most common type of construct in tissue engineering applications, engineered surfaces are also important [57, 58]. Often ECM like collagen is used to make materials like titanium for implants biocompatible [59]. Knowing the best approach by which to attach collagen or other ECM to the surface in order for the body to populate it with the appropriate cells that are either dispersed or clustered will have noticeable impact on the design of biomaterials like artificial hips and dental implants [60, 61].

## CONCLUSIONS:

We observed that MTLn3 cells formed clusters on physically adsorbed collagen substrates, while on covalently attached collagen surfaces, cells were more scattered. This clustering appears to be independent of cell-cell attachments as these cells make few due to their highly metastatic nature. We quantified several clustering parameters based on a radial distribution function and a *k*-means clustering approach and the quantification confirmed our qualitative observations. Cells on covalently attached collagen surfaces had larger peak distances and decay distances and resulted in lower percentage of cells in clusters. We found that surfaces with covalently attached collagen were more resistant to desorption of collagen than surfaces with adsorbed collagen. While proliferation was the same on physically adsorbed collagen in comparison to covalently attached collagen, the migration speed and persistence time were much lower resulting in clustering. This study shows that cell clustering, even in cells that make few cell-cell contacts, is regulated through ECM attachment and the modulation of cell migration characteristics.

This is a manuscript of an article from Physical Biology 11 (2014): 056007, doi: 10.1088/1478-3975/11/5/056007.
Posted with permission.

## ACKNOWLEDGMENTS:

The authors thank Mathew Constant for help in data analysis and Elizabeth Whitley for a helpful discussion.

The authors acknowledge support from the Roy J. Carver Charitable Trust (12-3939) for general project funding and from NSF ARI-R2 (CMMI-0963224) for funding the renovation of the research laboratories used for these studies.

## References:


[1] Thiery J P, Acloque H, Huang R Y J and Nieto M A 2009 Epithelial-Mesenchymal Transitions in Development and Disease *Cell* **139** 871-90

[2] Hanahan D and Weinberg R 2000 The hallmarks of cancer *Cell* **100** 57-70

[3] Sasai Y 2013 Cytosystems dynamics in self-organization of tissue architecture *Nature* **493** 318-26

[4] Ma P C, Maulik G, Christensen J and Salgia R 2003 c-Met: Structure, functions and potential for therapeutic inhibition *Cancer and Metastasis Reviews* **22** 309-25

[5] Zhang Y, Lu H, Dazin P and Kapila Y 2004 Squamous cell carcinoma cell aggregates escape suspension-induced, p53-mediated anoikis - Fibronectin and integrin alpha(v) mediate survival signals through focal adhesion kinase *Journal of Biological Chemistry* **279** 48342-9

[6] Zhang X, Xu L H and Yu Q 2010 Cell aggregation induces phosphorylation of PECAM-1 and Pyk2 and promotes tumor cell anchorage-independent growth *Molecular Cancer* **9** 11

[7] Vincent-Salomon A and Thiery J 2003 Host microenvironment in breast cancer development - Epithelial-mesenchymal transition in breast cancer development *Breast Cancer Research* **5** 101-6

[8] Wei C, Larsen M, Hoffman M P and Yamada K M 2007 Self-organization and branching morphogenesis of primary salivary epithelial cells *Tissue Engineering* **13** 721-35

[9] Moscona A and Moscona H 1952 The dissociation and aggregation of cells from organ rudiments of the early chick embryo *Journal of Anatomy* **86** 287-&

[10] Giudice G 1962 Restitution of whole larvae from disaggregated cells of sea urchin embryos *Developmental Biology* **5** 402-&

[11] Ferrari C, Balandras F, Guedon E, Olmos E, Chevalot I and Marc A 2012 Limiting Cell Aggregation During Mesenchymal Stem Cell Expansion on Microcarriers *Biotechnology Progress* **28** 780-7

[12] Guaita S, Puig I, Franci C, Garrido M, Dominguez D, Batlle E, Sancho E, Dedhar S, de Herreros A G and Baulida J 2002 Snail induction of epithelial to mesenchymal transition in tumor cells is accompanied by MUC1 repression and ZEB1 expression *Journal of Biological Chemistry* **277** 39209-16

[13] Grotegut S, von Schweinitz D, Christofori G and Lehembre F 2006 Hepatocyte growth factor induces cell scattering through MAPK/Egr-1-mediated upregulation of Snail *Embo Journal* **25** 3534-45

[14] Boyer B, Roche S, Denoyelle M and Thiery J P 1997 Src and Ras are involved in separate pathways in epithelial cell scattering *Embo Journal* **16** 5904-13

[15] Khwaja A, Lehmann K, Marte B M and Downward J 1998 Phosphoinositide 3-kinase induces scattering and tubulogenesis in epithelial cells through a novel pathway *Journal of Biological Chemistry* **273** 18793-801

[16] de Rooij J, Kerstens A, Danuser G, Schwartz M A and Waterman-Storer C M 2005 Integrin-dependent actomyosin contraction regulates epithelial cell scattering *The Journal of Cell Biology* **171** 153-64

[17] Ryan P, Foty R, Kohn J and Steinberg M 2001 Tissue spreading on implantable substrates is a competitive outcome of cell-cell vs. cell-substratum adhesivity *Proceedings of the National Academy of Sciences of the United States of America* **98** 4323-7

[18] Montesano R, Matsumoto K, Nakamura T and Orci L 1991 Identification of a fibroblast-derived epithelial morphogen as hepatocyte growth-factor *Cell* **67** 901-8

[19] Pope M, Graham N, Huang B and Asthagiri A 2008 Automated quantitative analysis of epithelial cell scatter *Cell Adhesion & Migration* **2** 110-6



This is a manuscript of an article from Physical Biology 11 (2014): 056007, doi: 10.1088/1478-3975/11/5/056007.
Posted with permission.

[20] Guo W H, Frey M T, Burnham N A and Wang Y L 2006 Substrate rigidity regulates the formation and maintenance of tissues *Biophys. J.* **90** 2213-20
[21] Guvakova M A and Surmacz E 1997 Overexpressed IGF-I receptors reduce estrogen growth requirements, enhance survival, and promote E-cadherin-mediated cell-cell adhesion in human breast cancer cells *Experimental Cell Research* **231** 149-62
[22] Saez A, Anon E, Ghibaudo M, du Roure O, Di Meglio J M, Hersen P, Silberzan P, Buguin A and Ladoux B 2010 Traction forces exerted by epithelial cell sheets *J. Phys.-Condes. Matter* **22**
[23] Ng M R, Besser A, Danuser G and Brugge J S 2012 Substrate stiffness regulates cadherin-dependent collective migration through myosin-II contractility *J. Cell Biol.* **199** 545-63
[24] Gassei K, Ehmcke J and Schlatt S 2008 Initiation of testicular tubulogenesis is controlled by neurotrophic tyrosine receptor kinases in a three-dimensional Sertoli cell aggregation assay *Reproduction* **136** 459-69
[25] Pope M D and Asthagiri A R 2012 Short-Lived, Transitory Cell-Cell Interactions Foster Migration-Dependent Aggregation *Plos One* **7**
[26] Mina-Osorio P, Shapiro L H and Ortega E 2006 CD13 in cell adhesion: aminopeptidase N (CD13) mediates homotypic aggregation of monocytic cells *Journal of Leukocyte Biology* **79** 719-30
[27] de la Rosa G, Yanez-Mo M, Samaneigo R, Serrano-Gomez D, Martinez-Munoz L, Fernandez-Ruiz E, Longo N, Sanchez-Madrid F, Corbi A L and Sanchez-Mateos P 2005 Regulated recruitment of DC-SIGN to cell-cell contact regions during zymosan-induced human dendritic cell aggregation *Journal of Leukocyte Biology* **77** 699-709
[28] Silver D L and Montell D J 2001 Paracrine signaling through the JAK/STAT pathway activates invasive behavior of ovarian epithelial cells in Drosophila *Cell* **107** 831-41
[29] Hardikar A A, Marcus-Samuels B, Geras-Raaka E, Raaka B M and Gershengorn M C 2003 Human pancreatic precursor cells secrete FGF2 to stimulate clustering into hormone-expressing islet-like cell aggregates *Proceedings of the National Academy of Sciences of the United States of America* **100** 7117-22
[30] Kudo T, Kigoshi H, Hagiwara T, Takino T, Yamazaki M and Yui S 2009 Cathepsin G, a neutrophil protease, induces compact cell-cell adhesion in MCF-7 human breast cancer cells *Mediators Inflamm* **2009** 850940
[31] Andl C D, Mizushima T, Nakagawa H, Oyama K, Harada H, Chruma K, Herlyn M and Rustgi A K 2003 Epidermal Growth Factor Receptor Mediates Increased Cell Proliferation, Migration, and Aggregation in Esophageal Keratinocytes in Vitro and in Vivo
[32] Wu Z, Yu Y, Zhang J, Zhai Y, Tao Y and Shi J 2013 Clustered immature myeloid precursors in intertrabecular region during remission evolve from leukemia stem cell near endosteum and contribute to disease relapse in acute myeloid leukemia *Medical hypotheses* **80** 624-8
[33] Shields M A, Dangi-Garimella S, Krantz S B, Bentrem D J and Munshi H G 2011 Pancreatic cancer cells respond to type I collagen by inducing snail expression to promote membrane type 1 matrix metalloproteinase-dependent collagen invasion *J Biol Chem* **286** 10495-504
[34] Shields M A, Krantz S B, Bentrem D J, Dangi-Garimella S and Munshi H G 2012 Interplay between β1-integrin and Rho signaling regulates differential scattering and motility of pancreatic cancer cells by snail and Slug proteins *J Biol Chem* **287** 6218-29
[35] Gilchrist C L, Darling E M, Chen J and Setton L A 2011 Extracellular Matrix Ligand and Stiffness Modulate Immature Nucleus Pulposus Cell-Cell Interactions *PLoS ONE* **6** e27170
[36] Salmenpera P, Kankuri E, Bizik J, Siren V, Virtanen I, Takahashi S, Leiss M, Fassler R and Vaheri A 2008 Formation and activation of fibroblast spheroids depend on fibronectin-integrin interaction *Experimental Cell Research* **314** 3444-52
[37] Rhee S, Ho C H and Grinnell F 2010 Promigratory and procontractile growth factor environments differentially regulate cell morphogenesis *Experimental Cell Research* **316** 232-44

This is a manuscript of an article from Physical Biology 11 (2014): 056007, doi: 10.1088/1478-3975/11/5/056007.
Posted with permission.

[38] da Rocha-Azevedo B, Ho C-H and Grinnell F 2013 Fibroblast cluster formation on 3D collagen matrices requires cell contraction dependent fibronectin matrix organization *Experimental Cell Research* **319** 546-55
[39] Xu R, Boudreau A and Bissell M 2009 Tissue architecture and function: dynamic reciprocity via extra- and intra-cellular matrices *Cancer and Metastasis Reviews* **28** 167-76
[40] Branch D W, Corey J M, Weyhenmeyer J A, Brewer G J and Wheeler B C 1998 Microstamp patterns of biomolecules for high-resolution neuronal networks *Med Biol Eng Comput* **36** 135-41
[41] Romsey N R, Hou Y, Rodriguez L L and Schneider I C 2014 The Number of Lines a Cell Contacts and Cell Contractility Drive the Efficiency of Contact Guidance *Cell. Mol. Bioeng.* **7** 122-35
[42] Edelstein A, Amodaj N, Hoover K, Vale R and Stuurman N 2010 *Computer Control of Microscopes Using μManager*: John Wiley & Sons, Inc.)
[43] Hou Y, Hedberg S and Schneider I C 2012 Differences in adhesion and protrusion properties correlate with differences in migration speed under EGF stimulation *BMC Biophys* **5** 8
[44] Othmer H G, Dunbar S R and Alt W 1988 Models of dispersal in biological systems *J Math Biol* **26** 263-98
[45] Dunn G A 1983 Characterising a kinesis response: time averaged measures of cell speed and directional persistence *Agents Actions Suppl* **12** 14-33
[46] Peruani F and Morelli L G 2007 Self-propelled particles with fluctuating speed and direction of motion in two dimensions *Phys. Rev. Lett.* **99**
[47] Schneider I C, Hays C K and Waterman C M 2009 Epidermal Growth Factor-induced Contraction Regulates Paxillin Phosphorylation to Temporally Separate Traction Generation from De-adhesion *Mol. Biol. Cell* **20** 3155-67
[48] Berlier J E, Rothe A, Buller G, Bradford J, Gray D R, Filanoski B J, Telford W G, Yue S, Liu J X, Cheung C Y, Chang W, Hirsch J D, Beechem J M, Haugland R P and Haugland R P 2003 Quantitative comparison of long-wavelength Alexa Fluor dyes to Cy dyes: Fluorescence of the dyes and their bioconjugates *J. Histochem. Cytochem.* **51** 1699-712
[49] Cuvelier D, Thery M, Chu Y S, Dufour S, Thiery J P, Bornens M, Nassoy P and Mahadevan L 2007 The universal dynamics of cell spreading *Curr. Biol.* **17** 694-9
[50] Douezan S, Guevorkian K, Naouar R, Dufour S, Cuvelier D and Brochard-Wyart F 2011 Spreading dynamics and wetting transition of cellular aggregates *Proceedings of the National Academy of Sciences of the United States of America* **108** 7315-20
[51] Douezan S, Dumond J and Brochard-Wyart F 2012 Wetting transitions of cellular aggregates induced by substrate rigidity *Soft Matter* **8** 4578-83
[52] Friedl P and Wolf K 2003 Tumour-cell invasion and migration: Diversity and escape mechanisms *Nat. Rev. Cancer* **3** 362-74
[53] Cavallaro U and Christofori G 2001 Cell adhesion in tumor invasion and metastasis: loss of the glue is not enough *Biochimica Et Biophysica Acta-Reviews on Cancer* **1552** 39-45
[54] Tomlinson J, Alpaugh M and Barsky S 2001 An intact overexpressed E-cadherin/alpha,beta-catenin axis characterizes the lymphovascular emboli of inflammatory breast carcinoma *Cancer Research* **61** 5231-41
[55] Kankuri E, Cholujova D, Comajova M, Vaheri A and Bizik J 2005 Induction of hepatocyte growth factor/scatter factor by fibroblast clustering directly promotes tumor cell invasiveness *Cancer Research* **65** 9914-22
[56] Lizonova A, Bizik J, Grofova M and Vaheri A 1990 Coexpresion of tumor-associated alpha-2-macroglobulin and growth-factors in human-melanoma cell-lines *Journal of Cellular Biochemistry* **43** 315-25
[57] Ma Z W, Mao Z W and Gao C Y 2007 Surface modification and property analysis of biomedical polymers used for tissue engineering *Colloids and Surfaces B-Biointerfaces* **60** 137-57

This is a manuscript of an article from Physical Biology 11 (2014): 056007, doi: 10.1088/1478-3975/11/5/056007.
Posted with permission.

[58] Bauer S, Schmuki P, von der Mark K and Park J 2013 Engineering biocompatible implant surfaces Part I: Materials and surfaces *Progress in Materials Science* **58** 261-326
[59] Morra M, Cassinelli C, Cascardo G, Cahalan P, Cahalan L, Fini M and Giardino R 2003 Surface engineering of titanium by collagen immobilization. Surface characterization and in vitro and in vivo studies *Biomaterials* **24** 4639-54
[60] Li Z X and Kawashita M 2011 Current progress in inorganic artificial biomaterials *Journal of Artificial Organs* **14** 163-70
[61] Puleo D A and Nanci A 1999 Understanding and controlling the bone-implant interface *Biomaterials* **20** 2311-21

## Figures:

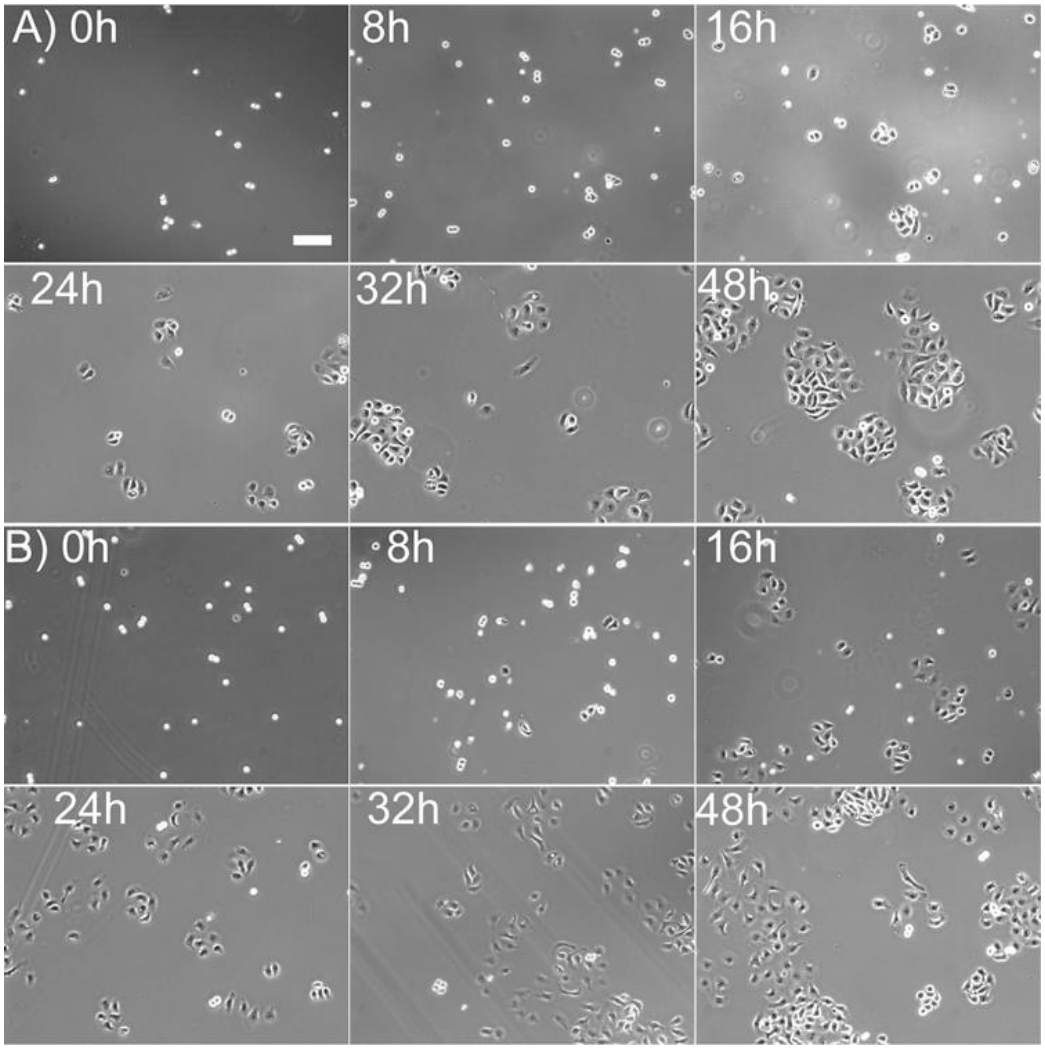


**Figure 1. Attachment mechanism of collagen produces differences in clustering in MTLn3 cells.** (*a*) Phys-COL and (*b*) Cov-COL substrates. Cells were imaged after incubation for 0, 8, 16, 24, 32 and 48 hrs in 5% serum α-MEM medium. Scale bar is 100 μm.

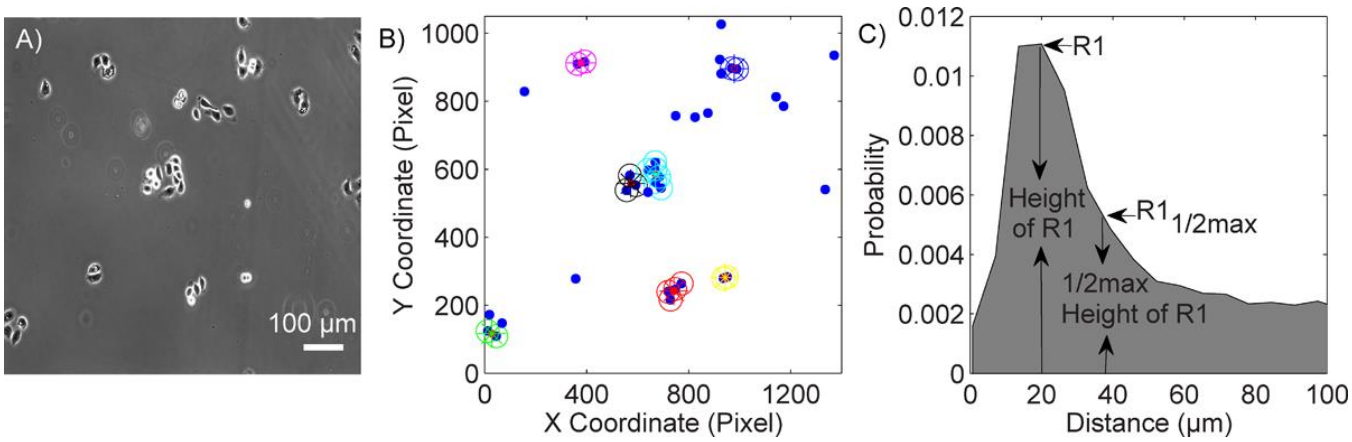


**Figure 2. Schematic illustrating cluster analysis.** (*a*) Original phase contrast image, (*b*) plot of cell and cluster positions and (*c*) plot of radial distribution function (RDF) showing peak distance (*R*) and decay distance ($R_{1/2max}$). The blue dots in (*b*) represent the centroids of cells in (*a*) and the different colored circles in (*b*) represent the cells in a cluster. The *asterisks* in (*b*) represent the centroids of clusters. Scale bar is 100µm.

This is a manuscript of an article from Physical Biology 11 (2014): 056007, doi: 10.1088/1478-3975/11/5/056007.
Posted with permission.

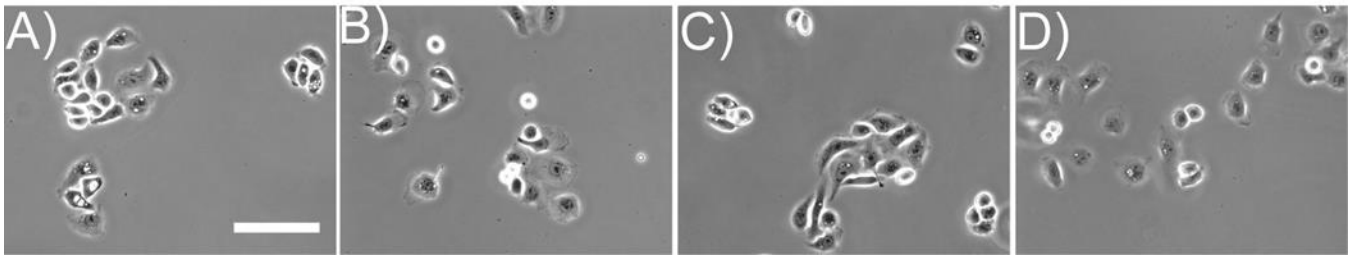


**Figure 3. PLL does not dramatically affect clustering on different substrates.** (*a*) Phys-COL, (*b*) Cov-COL, (*c*) Phys-COL+PLL and (*d*) Cov-COL+PLL. Cells were imaged after incubation for 24 h in 5% serum α-MEM medium. Scale bar is 100 μm.

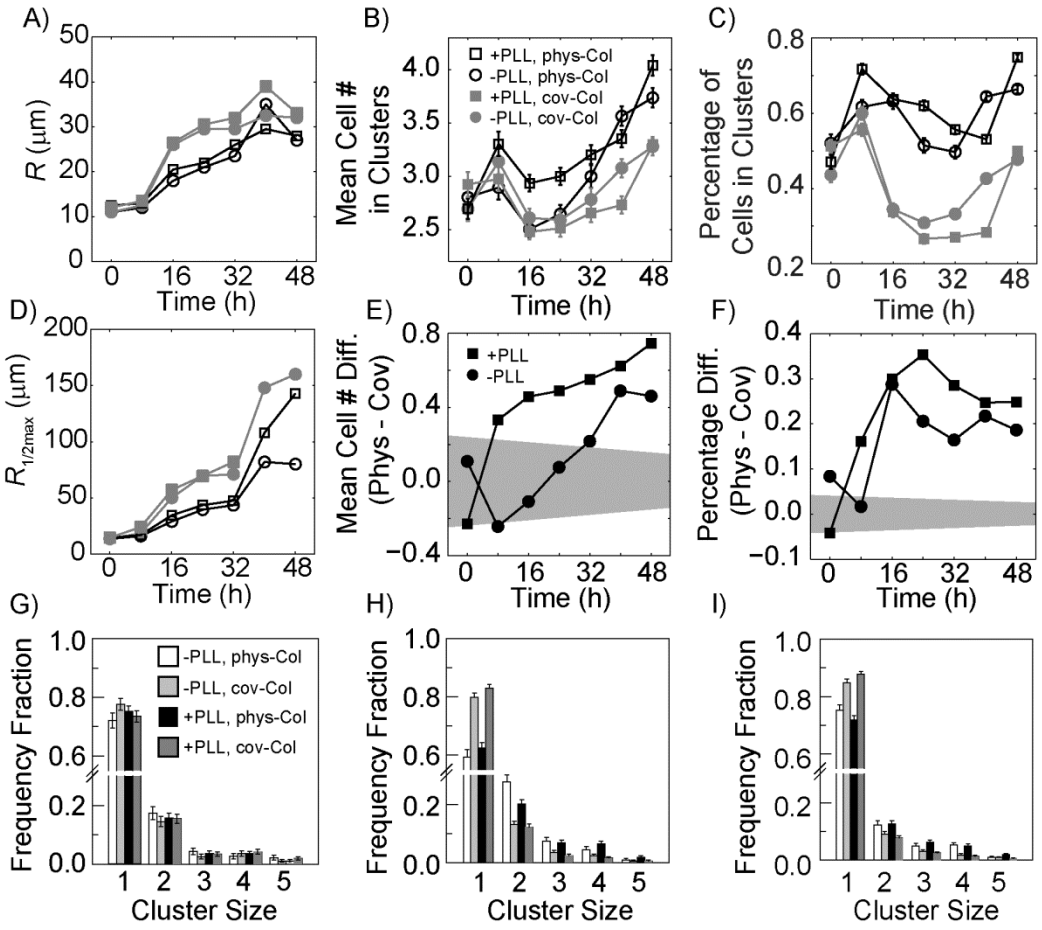


**Figure 4. Quantification of cell clustering over time on different substrates.** (*a*) Peak distance (*R*) of cells, (*b*) mean cell number in clusters, (*c*) percentage of cells in clusters (*d*) and decay distance ($R_{1/2max}$) are shown. The blackopen circle represents Phys-COL. The gray filled circle represents Cov-COL. The black open square represents Phys-COL+PLL. The gray filled square represents Cov-COL+PLL. The difference between the (*e*) mean cell number in clusters or (*f*) the percentage of cells in clusters for physically adsorbed and covalently attached conditions for both substrates lacking PLL (circle) and with PLL (square). The gray region denotes areas where the differences are not significant to 95% confidence. Example distributions for cluster sizes less than 5 cells at (*g*) 0 h, (*h*) 16 h and (*i*) 32 h. White/black bars are phyically adsorbed substrates and gray bars are covalently attached substrates. White and light gray bars represent substrates without PLL and black and dark gray bars representsubstrates with PLL. Error bars are 95% confidence intervals.

This is a manuscript of an article from Physical Biology 11 (2014): 056007, doi: 10.1088/1478-3975/11/5/056007.
Posted with permission.

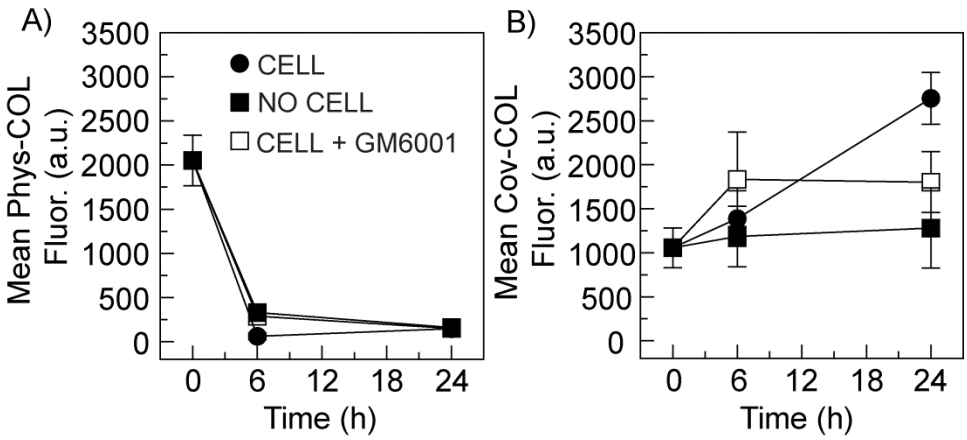


**Figure 5. Quantification of surface collagen density.** (*a*) Phys_COL and (*b*) Cov_COL. The black circles represent substrates with MTLn3 cells. The black squares represent substrates without cells. The open squares represent substrates with cells treated with an MMP inhibitor GM6001. Error bars are 95% confidence intervals.

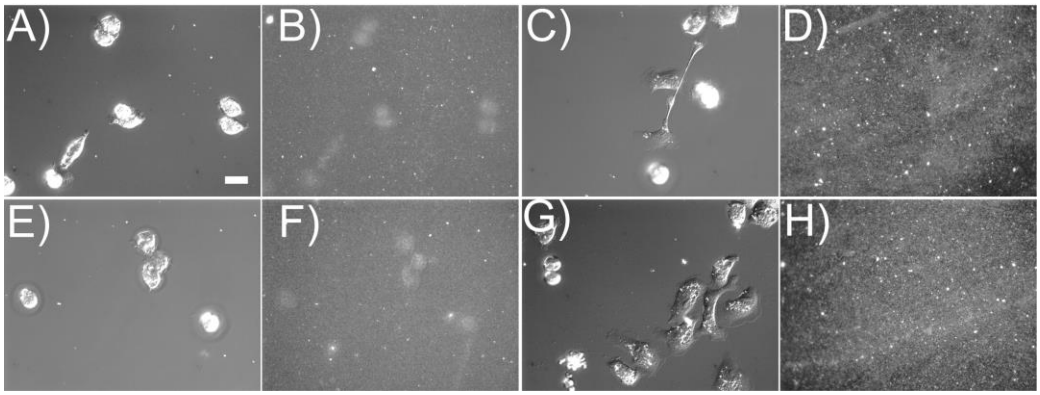


**Figure 6. Uptake of collagen by cells on different substrates.** (*a*) Differential interference contrast image of cells (*a*, *c*, *e* and *g*) and epifluorescence image of Alexa Fluor 555-labeled collagen (*b*, *d*, *f* and *h*) on Phys-COL (*a* and *b*), Cov-COL (*c* and *d*), Phys-COL+PLL (*e* and *f*) and Cov-COL+PLL (*g* and *h*). (*b*) and (*f*) as well as (*d*) and (*h*) were scaled to the same background level. Scale bar is 20 μm.

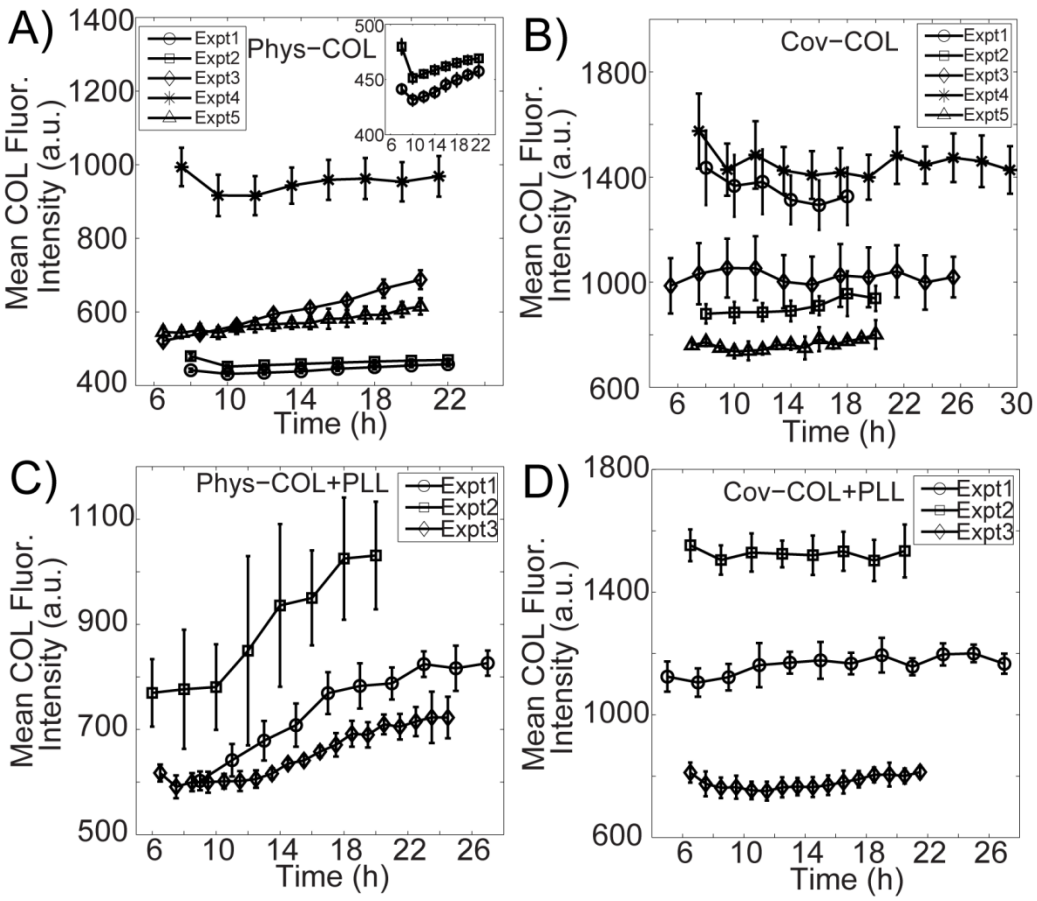


**Figure 7. Quantification of the uptake of collagen by cells on different substrates.** (*a*) Phys-COL, (*b*) Cov-COL, (*c*) Phys-COL+PLL and (*d*) Cov-COL+PLL. Different symbols and lines represent different experiments. Insert of (*a*) is the enlarged image of experiment 1 and 2 in (*a*). Error bars are 95% confidence intervals.

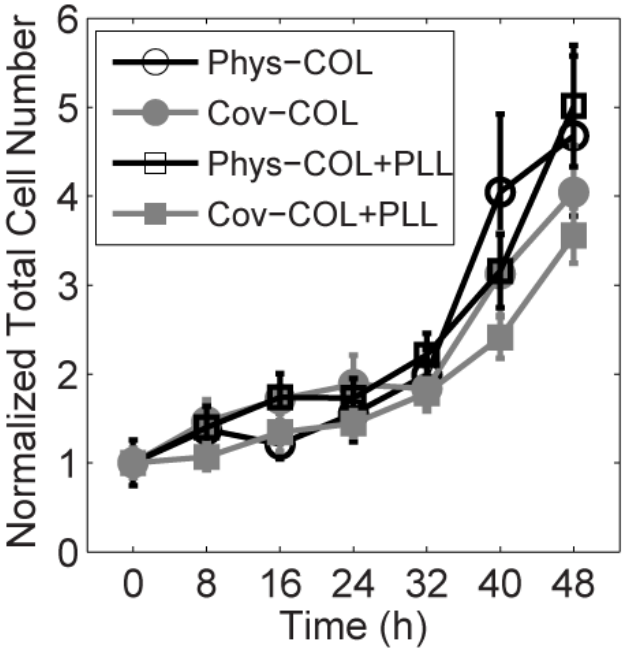


**Figure 8.Quantification of cell proliferation over time on different substrates.** Normalized total cell number was calculated. The black open circles represent Phys-COL. The gray filled circles represent Cov-COL. The black open squares represent Phys-COL+PLL. The gray filled squares represent Cov-COL+PLL. Error bars are 95% confidence intervals.

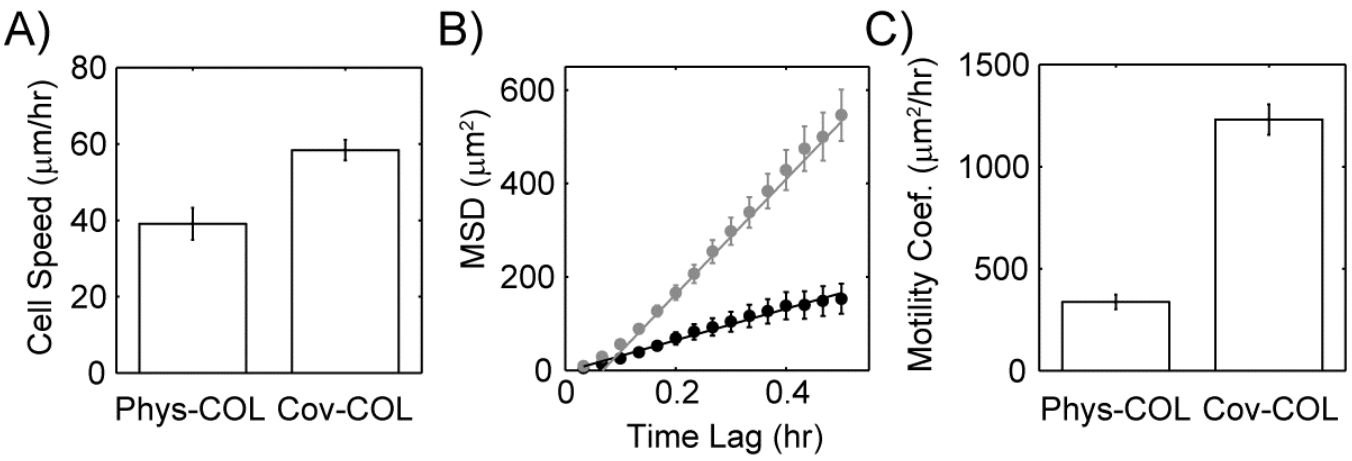


**Figure 9. Quantification of cell migration on different substrates.** Cells were tracked and motility characteristics were calculated. (*a*) Instantaneous cell speed was measured for cells plated on both Phys-COL and Cov-COL substrates. (*b*) The means squared displacement as a function of time lag for cells plated on both Phys-COL (black circles) and Cov-COL (gray circles). The long time behavior is fitted with a linear equation. (*c*) The motility coefficient is the slope of the linear fit of the long time behavior and is shown for both Phys-COL and Cov-COL substrates. Error bars represent 95% confidence intervals.

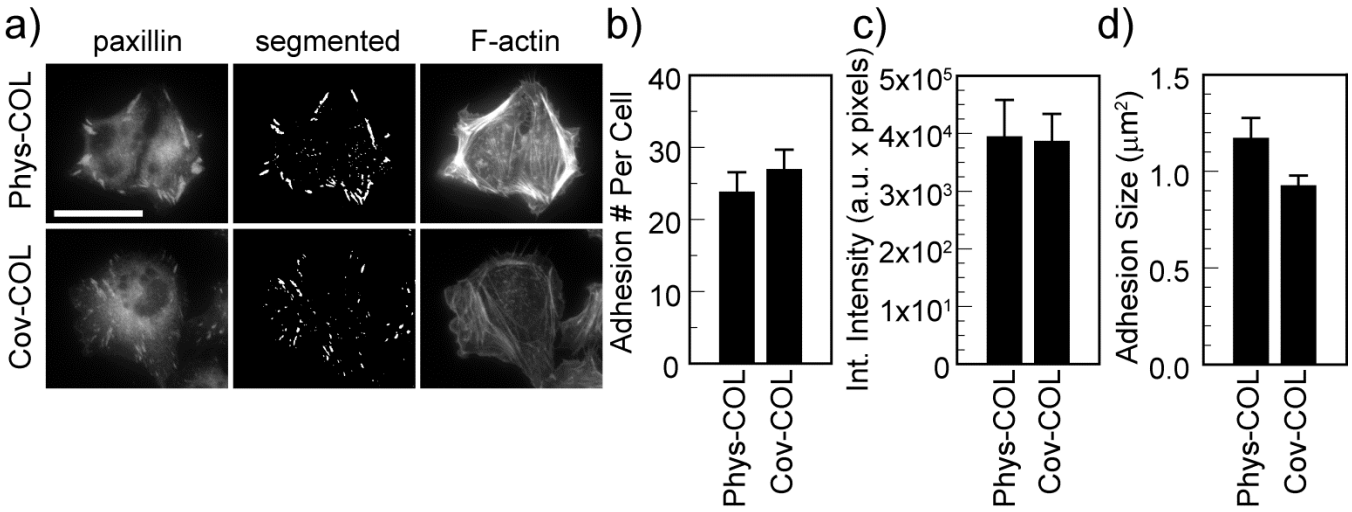


**Figure 10. Quantification of focal adhesion characteristics.** (*a*) MTLn3 cells were plated on Phys-COL and Cov-COL substrates for 16 h, fixed and stained for adhesions (paxillin) and the cytoskeleton (F-actin). Adhesions were segmented and (*b*) adhesion size, (*c*) number of adhesions per cell and (*d*) integrated intensity were quantified. The calibration bar is 30 μm and error bars represent 95% confidence intervals.

This is a manuscript of an article from Physical Biology 11 (2014): 056007, doi: 10.1088/1478-3975/11/5/056007.
Posted with permission.

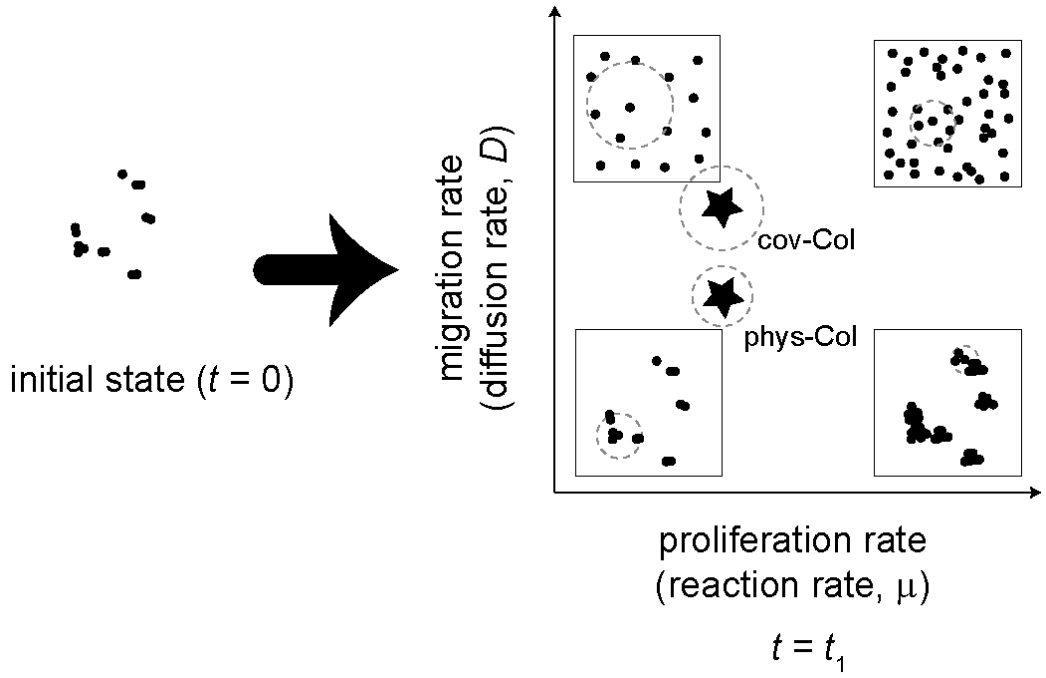


**Figure 11. Schematic of the balance between migration and proliferation rates.** Cells (black dots) are shown at the time of plating ($t$ = 0) (far left). At $t = t1$ (far right) a graph containing axes for migration rate (characterized by a diffusion coefficient) and proliferation rate (characterized by a reaction rate constant) is shown with schematics demonstrating the distributions of cells under different conditions in different parts of the graph. Cells for each condition are contained within a box. Gray dashed lines designate the characteristic cluster radius ($R$ or $R_{1/2max}$). Conditions are as follows: low proliferation and migration rates (lower left), high migration rate and low proliferation rate (upper left), low migration rate and high proliferation rate (lower right), proportionally higher migration and proliferation rates (upper right). The position on the graph for cells plated on covalently attached collagen and physically adsorbed collagen are shown as the stars, with the corresponding characteristic cluster radius shown in dashed gray lines.

This is a manuscript of an article from Physical Biology 11 (2014): 056007, doi: 10.1088/1478-3975/11/5/056007.
Posted with permission.

## Supplemental Figures:

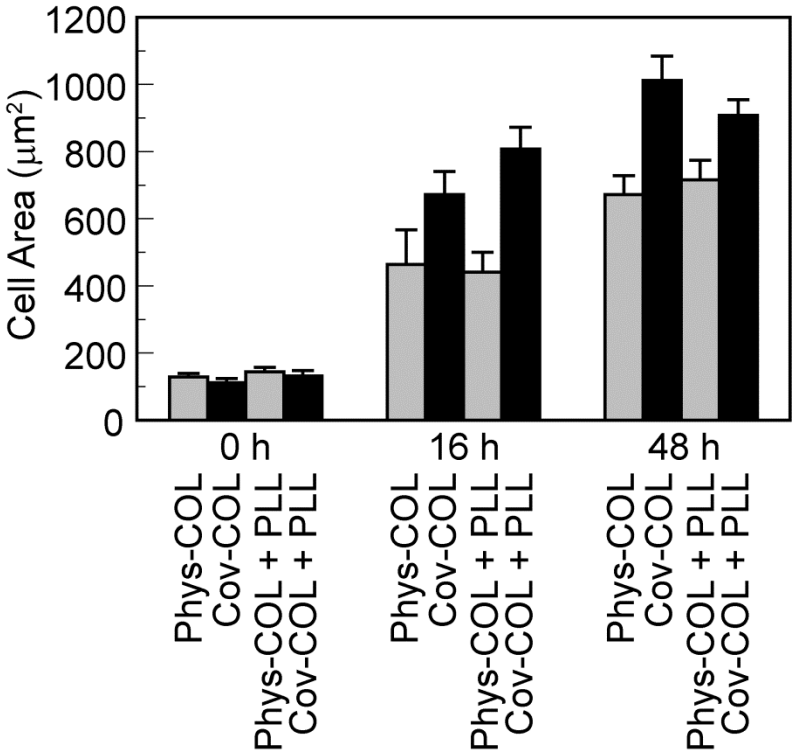


**Figure S1. Quantification of cell spreading on different substrates.** Cell spreading was measured at 0, 16 and 48 h under the different coating conditions from phase contrast images. The gray bars represents Phys-COL and the black bars represent Cov-COL. Error bars are 95% confidence intervals.

This is a manuscript of an article from Physical Biology 11 (2014): 056007, doi: 10.1088/1478-3975/11/5/056007.
Posted with permission.

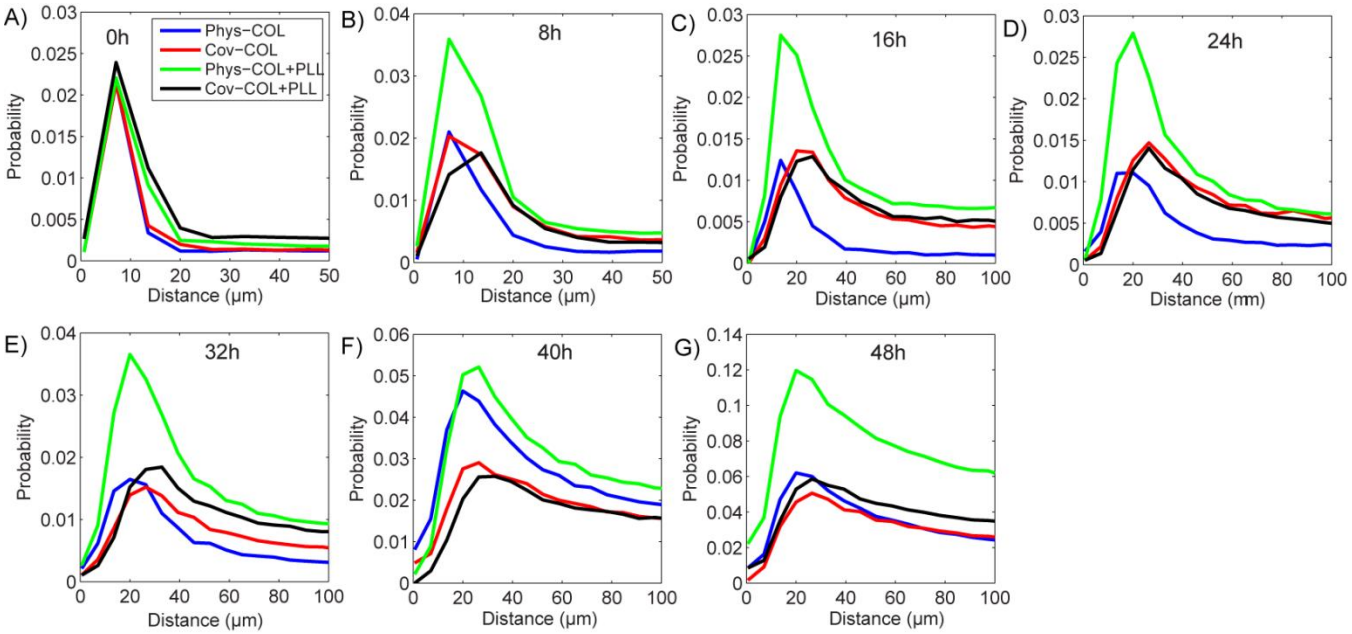


**Figure S2. Radial distribution functions of cells on different substrates at different time points.** (*a*) 0 h, (*b*) 8 h, (*c*) 16 h, (*d*) 24 h, (*e*) 32 h, (*f*) 40 h and (*g*) 48 h. The blue line represents Phys-COL. The red line represents Cov-COL. The green line represents Phys-COL+PLL. The black line represents Cov-COL+PLL.

This is a manuscript of an article from Physical Biology 11 (2014): 056007, doi: 10.1088/1478-3975/11/5/056007.
Posted with permission.

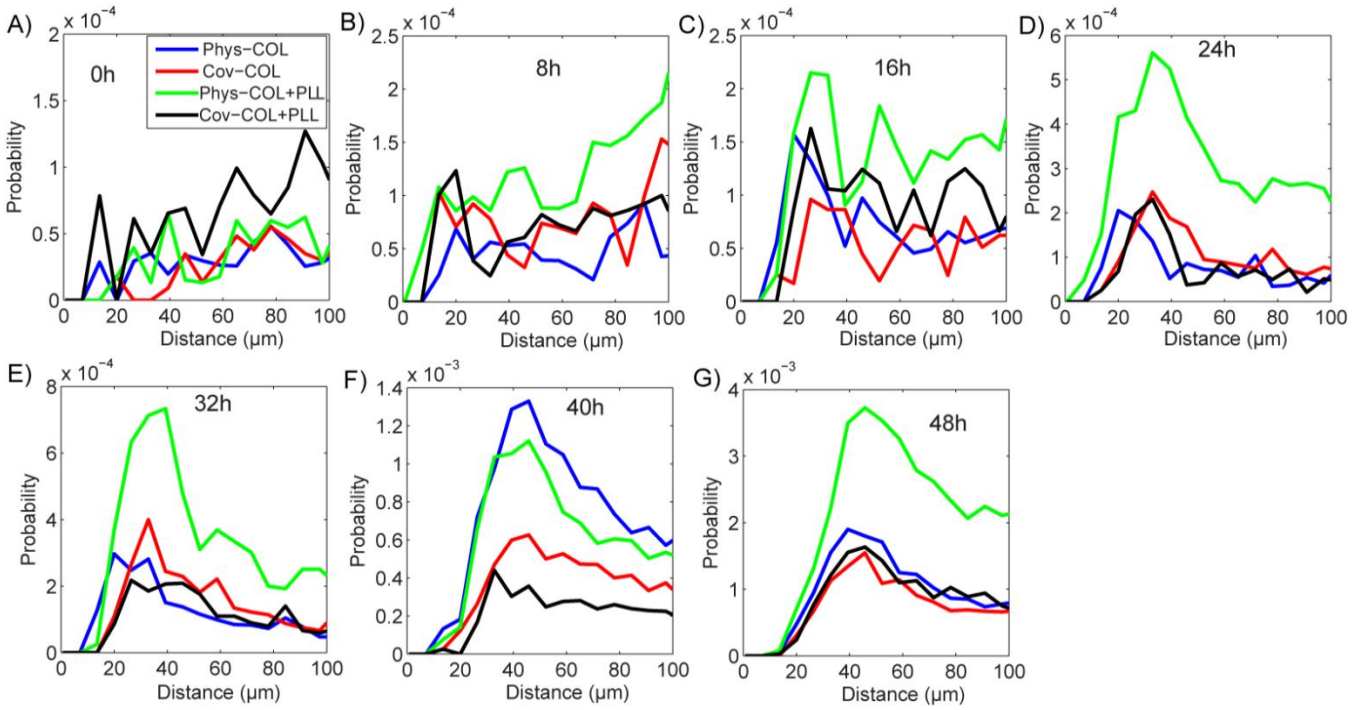


**Figure S3. Radial distribution functions of clusters on different substrates at different time points.** (*a*) 0 h, (*b*) 8 h, (*c*) 16 h, (*d*) 24 h, (*e*) 32 h, (*f*) 40 h and (*g*) 48 h. The blue line represents Phys-COL. The red line represents Cov-COL. The green line represents Phys-COL+PLL. The black line represents Cov-COL+PLL.

This is a manuscript of an article from Physical Biology 11 (2014): 056007, doi: 10.1088/1478-3975/11/5/056007.
Posted with permission.

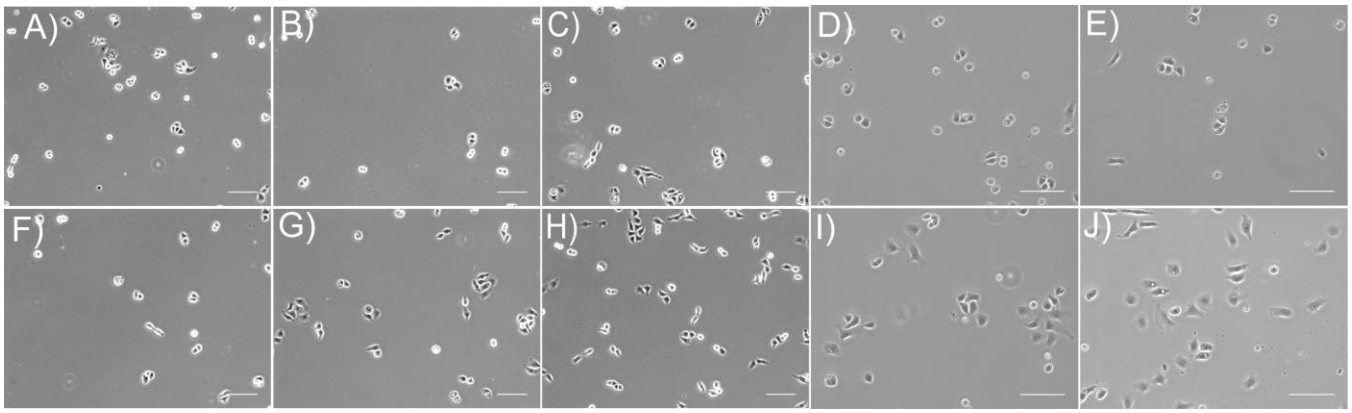


**Figure S4. Morphology of cells at 12-16h on different substrates.** (*a*) no COL Phys, (*b*) 0.3 µg/mL COL Phys, (*c*) 0.3 µg/mL COL+PLL Phys, (*d*) 30 µg/mL COL Phys, (*e*) stamped COL Phys, (*f*) no COL Cov, (*g*) 0.3 µg/mL COL Cov, (*h*) 0.3 µg/mL COL+PLL Cov, (*i*) 30 µg/mL COL Cov and (*j*) stamped COL Cov. Scale bar is 100 µm.